This is a preprint, the final version is subject to change, of the American Mineralogist (MSA)
Cite as Authors (Year) Title. American Mineralogist, in press.
DOI: https://doi.org/10.2138/am-2019-6559

Revision 3

Stability of the hydrous phases of Al-rich phase D and Al-rich phase H in deep subducted oceanic crust

Xingcheng Liu [12*], Kyoko N. Matsukage [23*], Yu Nishihara [4], Toshihiro Suzuki [2] and Eiichi Takahashi [12]

[1] *State Key Laboratory of Isotope Geochemistry, Guangzhou Institute of Geochemistry, Chinese Academy of Sciences, Wushan, Guangzhou 510640, P. R. China*

[2] *Magma Factory, Department of Earth and Planetary Sciences, Tokyo Institute of Technology, 2-12-1 Ookayama, Meguroku, Tokyo, 152-8551, Japan*

[3] *Center for Fundamental Education, Teikyo University of Science, 2525 Yatsuzawa, Uenohara City, Yamanashi, 409-0193, Japan*

[4] *Geodynamics Research Center, Ehime University, 2-5 Bunkyo-cho, Matsuyama City, Ehime 790-8577, Japan*

**E-mails: liuxingcheng@gig.ac.cn or matsukage@ntu.ac.jp*

ABSTRACT

To understand the stability of hydrous phases in mafic oceanic crust under deep subduction conditions, high-pressure and high-temperature experiments were conducted on two hydrous basalts using a Kawai-type multianvil apparatus at 17–26 GPa and 800–1200 °C. In contrast to previous studies on hydrous basalt that reported no hydrous phases in this pressure range, we found one or two hydrous phases in all run products at or below 1000 °C. Three hydrous phases, including Fe–Ti oxyhydroxide, Al-rich phase D and Al-rich phase H, were

present at the investigated P–T conditions. At T ≤ 1000 °C, Fe–Ti oxyhydroxide is stable at 17 GPa, Al-rich phase D is stable at 18–23 GPa, and Al-rich phase H is stable at 25-26 GPa. Our results, in combination with published data on the stability of hydrous phases at lower pressures, suggest that a continuous chain of hydrous phases may exist in subducting cold oceanic crust (≤ 1000 °C): lawsonite (0–8 GPa), Fe–Ti oxyhydroxide (8–17 GPa), Al-rich phase D (18–23 GPa), and Al-rich phase H (>23 GPa). Therefore, in cold subduction zones, mafic oceanic crust, in addition to peridotite, may also carry a substantial amount of water into the mantle transition zone and the lower mantle.

Keywords: Water, mantle transition zone, lower mantle, cold subduction, hydrous phases, basaltic crust

INTRODUCTION

The distribution of water in the mantle and its effect on mantle dynamics are important for understanding the evolution of the Earth. It is widely believed that subducting plates transport water from the surface into the deep mantle via a variety of hydrous phases in the subducting oceanic lithosphere (Hacker, 2008; Nishi et al. 2014; Ohira et al. 2014; Ohtani, 2015; Pamato et al. 2015). The stability of hydrous phases, under conditions of plate subduction, has been studied extensively (e.g., Kawamoto, 2006; Melekhova et al. 2007; Walter et al. 2015). Experiments in simple systems and in multicomponent peridotite-H_2O systems demonstrated that phase D ($MgSi_2H_2O_6$) is stable to pressures up to 44 GPa and temperatures up to 1800 °C, and this phase is proposed as a major water carrier into the lower mantle (Frost and Fei, 1998; Ohtani et al. 2000; Litasov et al. 2007; 2008; Ballaran et al., 2010; Ghosh and Schmidt, 2014; Pamato et al.

2015; Nishi et al. 2014; Walter et al. 2015). Furthermore, in basalt-H_2O systems, early experimental investigations did not observe any hydrous phases that can be stable above 10 GPa (Litasov and Ohtani, 2005; Okamoto and Maruyama, 1999; 2004); thus, mafic oceanic crust was considered unimportant as a water carrier. Recently, Nishihara and Matsukage (2016) reported a new hydrous phase, Fe–Ti oxyhydroxide, which is stable in hydrous basalt at pressures >10 GPa. These authors pointed out that mafic oceanic crust is a potential water carrier in the deep mantle. Pamato et al (2015) also mentioned that the relatively high Al contents of oceanic crust could expand the stability field of hydrous phases over that observed in peridotite systems, implying hydrous recycled oceanic crust could be a long-term water reservoir in the deep mantle. In this study, we performed high-pressure and high-temperature experiments with hydrous basalts at 17–26 GPa and 800–1200 °C. We found that three hydrous phases, including Fe–Ti oxyhydroxide, Al-rich phase D, (Mg, Fe)$(Si_{1-x}, Al_x)_2H_{2+2x}O_6$ (x=0.13–0.40), and Al-rich phase H, $Mg_{0.11}Fe_{0.03}Si_{0.2}Al_{0.63}HO_2$, are stable under the experimental conditions. These results provide the possibility that water can be accommodated in these hydrous phases in subducting oceanic crusts. Therefore, the subducted oceanic crust may transport more water into the lower mantle than previously thought.

EXPERIMENTAL METHODS

Two basaltic starting materials (Table 1), an olivine tholeiite JB-2* (hydrated JB-2) and an N-MORB, with 12.0 wt% and 8.3 wt% MgO, respectively, were used in this work. The first was prepared from a mixed powder of JB-2—a natural basalt-standard rock and collected by the Geological Survey of Japan (Ando et al. 1989)—and brucite, in a mass ratio of 89:11. This mixture produced an H_2O content of 3.5 wt%. The second was a hydrous N-MORB glass (~2.0

wt% H_2O), synthesized at 0.4 GPa and 1200 °C using a gas-medium apparatus. Each starting material was ground in acetone over an hour to improve the chemical homogeneity and then placed in an oven at 110 °C to remove moisture. Au–Pt double capsules were used as sample containers. For the runs at $P \leq 20$ GPa, the starting material in each run was loaded into an inner Au capsule (1.3 mm OD, 1.1 mm ID and 1.5 mm length), and the oxygen fugacity was controlled at the ~NNO buffer, with a $NiO + Ni + Ni(OH)_2$ powder, which occupied the space between this inner Au capsule and an outer Pt capsule (1.6 mm OD, 1.4 mm ID and 2.5 mm length). Two thin Pt discs were placed between the buffer and the Au capsule to reduce possible reaction between them (see Fig. 1). For the runs at $P > 20$ GPa, it was difficult to employ the double capsule technique due to much smaller size of furnace. Thus, a simple Au capsule without an oxygen fugacity buffer was used at $P > 20$ GPa. For these experiments, the oxygen fugacity may be controlled by the starting material, which is close to ΔFMQ, based on the Fe^{3+}/Fe^{2+} ratio of the starting material (see Table 1). All capsules were sealed by arc welding.

High-pressure and high-temperature experiments were conducted with the two hydrous basalts at 17–26 GPa and 800–1200 °C using a Kawai-type multianvil UHP-2500 at the Magma Factory, Tokyo Institute of Technology. Tungsten carbide anvils with truncated edge lengths of 5 and 3 mm were used in combination with a Cr-doped MgO octahedral pressure medium, with 10- and 8-mm edge lengths in experiments at $P \leq 20$ GPa and > 20 GPa, respectively. Pyrophyllite gaskets were employed to support the anvil flanks. Cylindrical $LaCrO_3$ was used as a heater, and the temperature was monitored by a 0.125-mm diameter $W_{95}Re_5$–$W_{74}Re_{26}$ C-type thermocouple. The cell-assembly for experiments conducted at $P \leq 20$ GPa is shown in Fig. 1. These gold sample capsules were believed to have been located in the hotspots of the furnace.

Pressure was calibrated based on the phase transitions of Bi (I–II), ZnS, GaAs, and GaP at room temperature, and based on SiO_2 (coesite–stishovite), olivine (α-β and β-γ), and $MgSiO_3$ (ilmenite–perovskite) at 1600 °C (Katsura et al., 2004; Matsuzaka et al., 2000; Zhang et al., 1996). The experiments were initially pressurized to each target pressure at room temperature and subsequently heated to the target temperature at a rate of 50 °C/min. Run durations ranged from 12 to 50 hours, depending on the run temperature. All the experiments were quenched by switching off the electricity to the heater. The recovered sample capsules were mounted in epoxy resin and carefully polished.

ANALYTICAL METHODS

Run products were analyzed with on a JEOL-JXA8530F field emission electron probe microanalyzer housed at the ELSI, Tokyo Institute of Technology. Microanalysis was performed in WDS mode. A focused beam (1 μm) was used. The voltage was 15 kV, and the beam current was 10 nA for silicate minerals and 1 nA for hydrous phases. The employed standards were wollastonite (Ca, Si), hematite (Fe), periclase (Mg), corundum (Al), albite (Na), aduralia (K), rutile (Ti), Cr_2O_3 (Cr), bunsenite (Ni), and tephroite (Mn). Counting times were 20 s for peak measurement and 10 s for background for all elements, except for Na and K, which had 10 s for peak and 5 s for background.

X-ray diffraction (XRD) analyses were performed using a micro-focused X-ray diffractometer RIGAKU RINT RAPIDII installed at GRC Ehime University for phase identification. This diffractometer is equipped with a rotative anode (Cu*K*α radiation), a two-dimensional imaging plate detector and a ϕ100 μm collimator. The operating conditions were 40

115 kV, 30 mA, and an exposure time in the XRD analyses was 300 s. Diffraction patterns were
116 collected in the 2θ range from 20 to 155°. Phase identification was carried out using the software
117 PDIndexer. Selected XRD patterns of run products are shown in Fig. 2. We used XRD patterns
118 only for phase identification because many diffraction peaks of coexisting phases were generally
119 overlapped and precise determination of lattice parameters was difficult.
120
121 **RESULTS**
122 **Phase relations and chemical compositions**
123 Fourteen experiments were conducted. Synthesized phase assemblages include majoritic
124 garnet, Ca-perovskite, stishovite, K-hollandite, ringwoodite, magnesiowustite, bridgmanite,
125 hydrous phases and fluids (Table 2). Except for two runs at a temperature of 1200 °C and
126 pressures of 17 and 19 GPa, the hydrous phases were observed in all the run products. Chemical
127 compositions and proportions of each phases are presented in Supplementary Table 1S. The
128 proportions are based on mass balance calculations. Back-scattered electron images of
129 representative run products are shown in Fig. 3. The detailed description on the synthesized
130 phases is as followed.
131
132 **Majoritic garnet and bridgmanite**
133 Majoritic garnet occurred as the major phase in experiments at pressures ≤ 23 GPa. In the
134 garnets, Al_2O_3 content increases, but the CaO content decreases, with increasing pressure (see
135 Supplementary Table 1S). For example, at 17–23 GPa and 1000 °C, the Al_2O_3 content in garnet
136 increases from 15.5 to 20.0 wt%, and the CaO content decreases from 9.5 to 3.3 wt%. This
137 observation is consistent with a previous experimental study using hydrous basalt by Litasov and

Ohtani (2005). The modal proportions of hydrous phases depend mainly on the proportion of the coexisting garnet. The proportion of garnet can be over 75 wt% in the run products without Al-rich phase D (such as DHL-1, DHL-4 and DHL-19). By contrast, the amount of garnet shrank as the amount of Al-rich phase D increased. Similarly, the decline of CaO content in garnet results in increasing proportions of Ca-perovskite in the run products.

At pressures ≥ 25 GPa, bridgmanite occurred as the major phase instead of garnet. As suggested by Hirose et al. (2005), garnet converts to Al-bearing bridgmanite and Ca-perovskite under lower mantle conditions. No systematic variation of bridgmanite composition was observed. However, the recovered bridgmanite is similar to compositions expected within subducted basalts (e.g., Hirose et al. 2005; Pamato et al. 2015). The bridgmanites in this study contain 10.2 to 11.9 wt% Al_2O_3, which is lower than that in the previous experimental study (~15.6 wt%) using hydrous basalt reported by Litasov and Ohtani (2005). The absence of Al-rich phase H in their run products may be responsible for the higher Al_2O_3 content in their bridgmanite.

Fe–Ti oxyhydroxide

In this study, Fe–Ti oxyhydroxide was present in experiments at P < 19 GPa and T = 900–1100 °C. This phase contains 47.2–59.4 wt% FeO_{total}, 6.9–14.3 wt% TiO_2 and approximately 16-17 wt% water (estimated from deficits in microprobe totals), which is similar to the hydrous phase investigated by Nishihara and Matsukage (2016). The water content of Fe–Ti oxyhydroxide in their study was estimated to be ~10 wt%. These authors demonstrated that the iron-rich solid solution has a ε-FeOOH type crystal structure, whereas the titanium-rich solid

161 solution has a α-PbO_2 type crystal structure. The ε-FeOOH type was found only at relatively low
162 temperature (<1100 °C) in their experiments. In this study, the Fe–Ti oxyhydroxide has a
163 composition closer to the Fe-rich end-member, then it has a lower temperature stability.
164
165 **Al-rich phase D and Al-rich phase H**
166 We have observed Al-rich phase D in the experiments performed at 18–25 GPa and Al-rich
167 phase H at 25–26 GPa. These hydrous phases were confirmed by X-ray diffraction patterns of
168 the run products (Fig. 2). The Al-rich phase D synthesized in this study contains 39.5–54.3 wt%
169 SiO_2, 7.5–22.6 wt% Al_2O_3, 3.4–5.4 wt% FeO_{total}, 16.1–20.6 wt% MgO, 11–15 wt% H_2O
170 (estimated from EMPA) and other minor elements. The (Mg+Fe)/Si and Al/Fe ratios are 0.64–
171 0.75 and 2.30–9.44, respectively (Supplementary Table 2S). The Al/Fe ratio in the Al-rich phase
172 D increases with increasing pressure and decreasing temperature and is much higher than those
173 observed in Fe, Al-poor compositions, consistent with the observation of Pamato et al. (2015). At
174 a given pressure, the Al_2O_3 content in Al-rich phase D decreases with increasing temperature,
175 whereas higher pressure enhances its Al_2O_3 and water content (Fig. 4 and Supplementary Tables
176 2S). The observed correlation between Al_2O_3 content and H_2O content in Al-rich phase D may
177 have resulted from substitution, i.e., $Al^{3+} + H^+ \leftrightarrow Si^{4+}$ (Fig. 5). However, for a given starting
178 composition at a given pressure, Pamato et al. (2015) found that the Al content in Al-rich phase
179 D increased with increasing temperature in their experiments, whereas the water content
180 decreased.
181
182 The formula of Al-rich phase D in our study is (Mg, Fe)$(Si_{1-x}, Al_x)_2H_{2+2x}O_6$, with x=0.13–
183 0.40. The composition is very similar to the Al-rich phase D synthesized by Bindi et al. (2015) at

184 45 GPa and 1000 °C and by Ghosh and Schmidt (2014) at 22–32 GPa and 1300–1450 °C with
185 MgO-SiO_2-Al_2O_3-H_2O as the staring material (Fig. 5), except that our Al-rich phase D contains
186 higher Al_2O_3 (Fig. 5). In recent experiments performed using simplified chemical systems
187 (Ghosh and Schmidt, 2014), the compositions of Al-rich phase D did not vary systematically
188 with pressure or temperature but did so according to the composition of the starting materials
189 (Fig. 5). Thus, we suggest that the variation of Al_2O_3 content in our Al-rich phase D synthesized
190 within a basaltic bulk composition may be controlled by the variation of phase assemblages and
191 their constituent proportions with increasing pressure, which is supported by changes in the
192 composition and proportions of other Al-bearing minerals, such as garnet (Supplementary Tables
193 1S).
194
195 The Al-rich phase H in this study has 18.3–20.6 wt% SiO_2, 52.3–53.0 wt% Al_2O_3, 3.5–3.8
196 wt% FeO_{total}, 6.9–7.5 wt% MgO, 15.8–17.1 wt% H_2O (estimated from EMPA) and other minor
197 elements. The formula of Al-rich phase H is $Mg_{0.11}Fe_{0.03}Si_{0.2}Al_{0.63}HO_2$. As shown in Fig. 4, the
198 compositions indicate that the Al-rich phase H synthesized herein was similar to the Al-rich end-
199 member of a solid solution between phase δ (AlOOH) and phase H ($MgSiH_2O_4$) (Ohira et al.
200 2014; Ohtani 2015; Suzuki et al. 2000). Although Bindi et al (2015) found the coexistence of Al-
201 rich phase D and Al-rich phase H at 45 GPa and 1000 °C, the Al-rich phase H in their study was
202 more likely the Al-poor end-member of a solid solution between phase δ (AlOOH) and phase H
203 ($MgSiH_2O_4$). In contrast with Bindi et al (2015), the Al-rich phase H contains much more Al
204 than Al-rich phase D in this study. Notably, the composition of Al-rich phase H was not
205 substantially affected by either temperature or pressure in this study.
206

The transformation from Al-rich phase D to Al-rich phase H has been observed in simplified chemical systems at P > 48 GPa, in which reactions of phase D + brucite ↔ phase H, and phase D ↔ phase H + stishovite were proposed by Nishi et al. (2014). Although this transformation was also observed in this study, we suggest that it may be a result of reaction of Al-rich phase D + garnet ↔ Al-rich phase H + bridgmanite + Ca-perovskite. Because bridgmanite has much lower Al_2O_3 contents than majoritic garnet, the Al_2O_3 from decomposition of garnet partitioned into Al-rich phase D to stabilize Al-rich phase H.

Minor phases

Calcium rich perovskite was formed in all experiments, except run DHL-6 (19 GPa and 800 °C). At pressures lower than 20 GPa, the Ti rich Ca-perovskite or (and) Ca-perovskite were formed as a minor phase. With increasing pressure, the proportion of Ca-perovskite increased up to 22 wt% as the garnet decomposed.

The experiments produced 2–10 wt% ringwoodite at 18–19 GPa. It should be noted that the ringwoodite in DHL-7 at 18 GPa and 900 °C has 8.9 wt% Na_2O as well as containing SiO_2, MgO and FeO (Supplementary Table 1S). Such Na-rich ringwoodite was also reported by Bindi et al. (2016), however, ringwoodite was not observed in hydrous basalts under similar conditions in previous experiments (Litasov and Ohtani, 2005; Okamoto and Maruyama, 2004). The occurrence of ringwoodite in this study may be due to higher MgO content (11.9 wt% MgO in JB-2* basalt) in the starting material compared to the MgO content in previous studies. Similarly, the high MgO in the starting material may also be responsible for the occurrence of magnesiowustite. Run DHL-8, which used JB-2*, produced magnesiowustite. In contrast, run

DHL-21 employed N-MORB (8.3 wt% MgO) as a starting material and did not yield magnesiowustite under the same P–T condition as that of DHL-8.

All experimental runs yielded stishovite. The Al_2O_3 content in stishovite increases from 0.3 to 1.6 wt% with increasing pressure, which is consistent with the observation by Litasov and Ohtani (2005). Unlike their experiments, our temperature range is relatively narrow; hence, no correlation between Al_2O_3 content in stishovite and temperature was found. The water content in stishovite, if any, ranges from 0 to 1 wt.%, which was estimated from deficits in the microprobe totals (see Table 1S).

The potassium hollandite was stable at P = 19–25 GPa and T < 1200 °C. This phase contains 63.9–67.0 wt% SiO_2, 18.0–19.3 wt% Al_2O_3 and 10.9–15.6 wt% K_2O and is a major potassium holder in the run products if present. No effect of pressure or temperature on the composition of hollandite was found.

DISCUSSION

Thermal gradient across the capsule

The stability of hydrous phases is sensitive to the temperature at a given pressure. Furthermore, the temperature at the capsule bottom (i.e., cold end) may be over 100 °C cooler than that at the top end (i.e., hot spot) if the capsule is longer than a few millimeters (e.g., Walter et al. 1995). Therefore, it is important to evaluate the thermal gradient across the capsule during the experiment.

Here, we estimate the thermal gradient via the distribution of hydrous phases in the runs at the same pressure but different temperatures. Although the distribution of hydrous phases is not simply controlled by the temperature at a given pressure in a hydrous experiment, we believe that the distribution of phases in subsolidus run products is mainly attributed to the thermal gradient. As shown in Fig. 6a, the sample capsule in DHL-5 (19 GPa and 1000 °C) was approximately 0.8 mm long, and Al-rich phase D was present from the top to the bottom. However, in DHL-19 (19 GPa and 1100 °C), Al-rich phase D was absent, and hydrous phase Fe-Ti oxyhydroxide appeared only at the bottom (Fig. 6b). If the vertical temperature variation in DHL-19 is greater than 100 °C, i.e., the temperature at the bottom is lower than 1000 °C, then Al-rich phase D should be stable and present at the bottom of DHL-19 as in DHL-5. It should be noted that Fe-Ti oxyhydroxide can coexist with Al-rich phase D, such as in DHL-18 (18 GPa and 900 °C). Therefore, we conclude that the thermal gradient in this study is smaller than 100 °C across a 0.8 mm long capsule. This conclusion (thermal gradient is less than 100 °C /0.8 mm) is supported by the systematics in hydrous phase stability of other run products. Relatively small temperature gradients in our run products may be due to the use of an Au capsule, which is a good heat conductor.

Stability field of hydrous phases in the hydrous basaltic system

To minimize the uncertainty in temperature, in the following discussion, we use phase assemblage (stability of hydrous phases) observed at the top portion of the capsule, within the 100 μm nearest to the thermocouple (e.g., DHL-5 in Fig. 6a). Therefore, the Fe–Ti oxyhydroxide in DHL-19 was not considered stable at 19 GPa and 1100 °C because it was present only at the cold end of the capsule (Fig. 6b). Similarly, a very small amount of Al-rich phase D (less than 1

276 wt.%) was observed only at the cold end of the capsule in DHL-15 and DHL-17, but it was not
277 considered to be stable hydrous phase at each experimental temperature. In this way, the stability
278 fields of hydrous phases were identified and plotted in Fig. 7, according to the experimental
279 conditions and stability of the hydrous phases near the thermocouple.
280
281 It should be noted that the stability filed of Al-rich phase D is sensitive to the bulk
282 composition (Ghosh and Schmidt, 2014; Pamato et al. 2015). Ghosh and Schmidt (2014)
283 reported that the addition of 1 wt% Al_2O_3 increases the stability field of phase D by 200 °C, but
284 this is an effect that is counter balanced by addition of 4.3 wt% FeO. Pamato et al. (2015) also
285 observed that increasing Al/Fe ratios in phase D expands its thermal stability. In this study, the
286 Al_2O_3 content in Al-rich phase D increases, and the FeO content remains constant with
287 increasing pressure. Although the stability of Al-rich phase D is smaller in basaltic systems than
288 that in MgO-FeO-SiO_2-Al_2O_3-H_2O simplified chemical systems, the higher Al_2O_3 content in
289 subducting oceanic crust may enhance the stability of Al-rich phase D and Al-rich phase H than
290 peridotite systems with much lower Al_2O_3 contents.
291
292 As depicted in Fig. 7, in the hydrous basaltic system, the hydrous phase is Fe–Ti
293 oxyhydroxide at pressures < 19 GPa and, at higher pressures, is a dense hydrous magnesium
294 silicate (DHMS), i.e., Al-rich phase D and Al-rich phase H. Al-rich phase D was stable between
295 19 GPa and 23 GPa and was replaced by Al-rich phase H at P > 25 GPa. The estimated water
296 contents in our synthesized Al-rich phase D and Al-rich phase H were 12–15 wt% and 16–17
297 wt%, respectively. Calculated proportions of solid phases in experimental run products (Table 2,
298 Supplementary Tables 1S) revealed that hydrous phases Al-rich phase D or Al-rich phase H

comprised ~16 wt% of each assemblage, which accommodated ~2.3 wt% water. This result reveals the critical role that oceanic crust can play as a water carrier into the transition zone or lower mantle.

Comparison with previous studies

The stability fields of hydrous phases synthesized in our work are shown in Fig. 7. We note that at least one hydrous phase was stable at ~1000 °C at all pressures considered, although none have been reported above 10 GPa in previous experiments performed on hydrous basalt (Litasov and Ohtani, 2005; Okamoto and Maruyama, 1999; 2004). Okamoto and Maruyama (1999; 2004) conducted experiments on MORB containing 2 wt% H_2O at 10–19 GPa and 700–1500 °C and reportedly lacked any hydrous phases; however, Nishihara and Matsukage (2016) noted that the Fe–Ti phase documented therein may have been Fe–Ti oxyhydroxide, which can hold up to 10 wt% H_2O. We also note that the experiments by Okamoto and Maruyama (1999; 2004) ran for 7 hours at 1000 °C (compared to 24 hours in our study), which may have been insufficient to stabilize crystals of Al-rich phase D large enough to analyze by EMPA.

Litasov and Ohtani (2005) investigated phase relations in hydrous MORB at 18–28 GPa and 1000–2400 °C using a starting material that was almost identical to that used in Okamoto and Maruyama (2004). The absence of hydrous phases in their study may be attributed to the use of a sample container comprised of an outer Pt capsule and an inner Re capsule, whereas we used an Au capsule for experiments conducted at >20 GPa and an Au–Pt double capsule and NNO buffer for experiments conducted at ≤20 GPa (Fig. 1). The rate of hydrogen diffusion under high-pressure and high-temperature conditions may be much faster in Pt and Re than in Au, causing

322 severe hydrogen depletion (i.e., water loss) during experimentation. In addition, the 1000 °C
323 experiments conducted by Litasov and Ohtani (2005) were preliminarily heated to 1200 °C for
324 two hours. During the preheating time, hydrogen loss from the Pt capsule may have accelerated
325 significantly. Hence, we infer that water loss or different experimental procedure may have led to
326 an absence of hydrous phases forming in their run products.
327
328 Alternatively, the contrasting result in hydrous phase stability between our study and those in
329 previous studies may be attributed to differences in the starting composition. Both of the
330 aforementioned studies (Litasov and Ohtani, 2005; Okamoto and Maruyama, 2004) used MORB,
331 which has 7.7 wt% MgO, whereas we used a basalt with 12 wt% MgO. Because Al-rich phase D
332 is MgO-rich, the higher MgO content of JB-2* may strongly affect its stability. To make clear
333 this point, we conducted an additional experiment (run DHL-21) using a hydrous N-MORB
334 containing 8.3 wt% MgO. A hydrous starting glass (2 wt% H_2O) was synthesized at 0.4 GPa and
335 1200 °C using a gas-medium apparatus, and experiments were carried out at 20 GPa using the
336 same double-capsule setup and techniques described above. Al-rich phase D was found to be
337 stable at 20 GPa and 1000 °C in the hydrous N-MORB (see Fig. 2, Table 2), although its
338 proportion was relatively smaller than that documented for the Mg-rich basalt starting material.
339 The difference between the run products in the present results and those from Litasov and Ohtani
340 (2005) might be explained by minor differences in compositions between the starting materials,
341 if it is not attributed to the water loss. The effect of the composition of the starting material needs
342 confirmation in future studies.
343
344 **The temperature of the subducting oceanic crust**

This is a preprint, the final version is subject to change, of the American Mineralogist (MSA)
Cite as Authors (Year) Title. American Mineralogist, in press.
DOI: https://doi.org/10.2138/am-2019-6559

Apparently, the top layer of a subducting slab is hotter than the interior, due to thermal diffusion from the ambient mantle (e.g., Syracuse et al. 2010). It is important to estimate the temperature of subducting oceanic crust while predicting the fate of water held in hydrous phases. The temperature of a subducting slab depends on several parameters. At a given mantle potential temperature, older subducting slabs with faster convergence rates are generally cooler than younger slabs with slower convergence rates (Magni et al. 2014). Thermomechanical modeling of 56 modern-day subduction zones has shown that slab-surface temperatures at a 240-km (i.e., 8 GPa) depth mainly lie in the range of 800–1000 °C (Syracuse et al. 2010). Extrapolation of these calculated thermal profiles to greater depths within the Earth (shaded area in Fig. 7) suggests that ~1000 °C is a reasonable estimation for the temperature in the uppermost 7 km of cold subducting oceanic crust under mantle transition zone conditions. Numerical simulations show that the core of such a thick slab at transition zone depths should have lower temperatures of 600–800 °C (King et al. 2015). Therefore, given a reasonable thermal structure within a cold subducting slab, either Al-rich phase D or Al-rich phase H would be stable in the oceanic crust (see phase proportion changes in Fig. 8), and DHMS would be stable in the peridotitic interior from the mantle transition zone to the uppermost lower mantle.

Implications for water transport into the mantle transition zone and lower mantle

Descending oceanic slabs mainly consist of peridotite and basalt on the top layer (oceanic crust, with average thickness of approximately 7 km). The hydrous phases in the hydrothermal metamorphic peridotitic system include serpentine and dense hydrous magnesium silicate (DHMS) with water contents of 3–18 wt%. However, none of them are stable at over approximately 8 GPa and characteristic slab temperature (Kawamoto, 2006). As demonstrated by

Kawamoto (2006), the choke point, therefore, is present in peridotite systems under down-going slab conditions, in which the hydrous phases get dehydrated and cannot deliver water to high pressure hydrous phases. Moreover, if we consider the dihedral angles of basalt and peridotite (i.e., the fluid connectivity of the rocks) at the choke point of peridotite, the fluids from the decomposition of hydrous phases in the peridotite would accumulate at the boundary of oceanic crust and peridotite in the subducting slab because the aqueous fluids can percolate through the peridotite part but not through the basaltic system (Kawamoto, 2006; Ono et al. 2002; Yoshino et al. 2007; Matsukage et al. 2017). According to our recent study (Liu et al, 2018), the dihedral angle within a basaltic system becomes less than 60 degrees above 14 GPa, thus water may percolate through both peridotite and basalt at temperatures above hydrous phase stability in cold subducted slabs.

Furthermore, our results show that a continuous chain of hydrous phases may exist in subducting, cold oceanic crust (~1000 °C): lawsonite (0–8 GPa); Fe–Ti oxyhydroxide (8–17 GPa); Al-rich phase D (18–22 GPa); and Al-rich phase H (>23 GPa). As mentioned above, the addition of Al_2O_3 and MgO expands the stability of Al-rich phase D. Therefore, it is probable that most of the Al-rich phase D (or Al-rich phase H at $P > 23$ GPa) occurs at the boundary between the oceanic crust and peridotite in the subducting slab. Al-rich phase H is known to be stable up to at least 128 GPa, 1900 °C (Ohira et al. 2014), indicating that subducting oceanic crust could transport water into the deepest parts of the lower mantle.

Global seismic tomography indicates that subducted slabs exhibit various behaviors at the upper mantle–lower mantle boundary (Fukao and Obayashi, 2013), such as the Pacific plate beneath China, which stagnates at the base of the upper mantle (~660 km), and those beneath the

Izu-Bonin-Mariana arc, which form a megalith and stagnate at ~1000 km depth (Fig. 9). The distribution of subducted oceanic crust in the stagnated megalith has been revealed via seismology (e.g., Kaneshima, 2003), and the temperature at the base of the upper mantle is estimated to be 1600–1700 °C (Akaogi et al. 1989). These stagnated slabs should thus be heated up by ambient, hot mantle over time, and thermal conduction calculations can be used to estimate when water would be liberated from the hydrous phases in both oceanic crust and peridotite. If a 100-km thick stagnant slab with a 7-km thick oceanic crust and a core temperature of 900 °C was subjected to an ambient mantle temperature of 1600 °C, the thermal stability of Al-rich phase H in basalt (1250 °C), which is located near the surface of the slab, and superhydrous phase B in peridotite (1400 °C), which may constitute the majority of the slab, would be exceeded within 10 Myr and 100 Myr, respectively, assuming thermal diffusivity of the rocks is 0.01 [cm^2/sec] (after Fig. 11.1-1 of Bird et al., 1960). Water would therefore be released from oceanic crust over a relatively shorter period (<10 Myr) than from peridotite (<100 Myr). Furthermore, dehydration from oceanic crust would take a much longer time if it is located inside the megalith, such as is shown in Fig. 9. Such dehydration can cause large-scale intracontinental magmas, such as those in China (e.g., Wang et al. 2015).

The importance of subducted oceanic crust as a water reservoir in the lower mantle has been recently discussed (Pamato et al. 2015). Our study sheds new light on the role of oceanic crust as a carrier of water during subduction by revealing the existence of a continuous chain of hydrous phases that can be stabilized from 10 GPa to 26 GPa. Mass-balance calculations performed on our run products between 20 GPa and 26 GPa show that MgO-rich basalt may contain up to 2 wt% H_2O at 1000 °C. According to the estimated changes in mantle potential temperature

414 throughout Earth's history, the average composition of oceanic crust may have evolved from
415 being high-MgO (komatiitic and/or picritic) on the early Earth to low-MgO (modern-day
416 MORB) today (Takahashi, 1990). Furthermore, Archaean oceanic crust was likely to have had a
417 thickness greater than 25 km; thus, the amount of water that could have been transported by
418 oceanic crust to the lower mantle may have been significantly greater in the geological past
419 (Palin and White, 2015).
420

421 **APPENDIX**

422 Supplementary Tables 1S and 2S are available online.

423 **ACKNOWLEDGMENTS**

424 This work is supported by the SPRP (B) from the Chinese Academy of Sciences (Grant No.
425 XDB18000000), Chinese Academy of Sciences (QYZDJ-SSW-DQC012, GIG135PY201601,
426 2017VSA0001) and JSPS (No. 25247088) to E.T. X.L. acknowledges a fund from NSFC (No.
427 41573053), National Key R&D Project of China (2016YFC0600104 and 2016YFC0600309) and
428 a one-year appointment as assistant professor at the Tokyo Institute of Technology. We are
429 grateful to Jennifer Kung and two anonymous reviewers for their careful and constructive
430 comments. We also thank Xiaolin Xiong and Tatsuhiko Kawamoto for discussion. This is
431 contribution No. XXX from GIGCAS.
432

REFERENCES CITED

Akaogi, M., Ito, E., and Navrotsky, A. (1989) Olivine‐modified spinel‐spinel transitions in the system Mg_2SiO_4‐Fe_2SiO_4: Calorimetric measurements, thermochemical calculation, and geophysical application, Journal of Geophysical Research: Solid Earth, 94(B11), 15671-15685.

Ando, A., Kamioka, H., Terashima, S., and Itoh, S. (1989) 1988 Values for Gsj Rock Reference Samples, Igneous Rock Series, Geochem J, 23(3), 143-148.

Ballaran, T.B., Frost, D.J., Miyajima, J.N., and Heidelbach, F. (2010) The structure of a super-aluminous version of the dense hydrous-magnesium silicate phase D, American Mineralogist, 95(7), 1113-1116.

Bindi, L., Nishi, M., and Irifune, T. (2015) Partition of Al between Phase D and Phase H at high pressure: Results from a simultaneous structure refinement of the two phases coexisting in a unique grain, American Mineralogist, 100(7), 1637-1640.

Bindi, L., Tamarova, A., Bobrov, A.V., Sirotkina, E.A., Tschauner, O., Walter, M.J., and Irifune, T. (2016) Incorporation of high amounts of Na in ringwoodite: Possible implications for transport of alkali into lower mantle, American Mineralogist, 101(1-2), 483-486.

Bird, R.B, Stewart, W.E., and Lightfoot, E.N. (1960) Transport Phenomena, Wiley International Edition, ISBN-10: 0470115394

Frost, D.J., and Fei, Y.W. (1998) Stability of phase D at high pressure and high temperature, Journal of Geophysical Research-Solid Earth, 103(B4), 7463-7474, doi:Doi 10.1029/98jb00077

Fukao, Y., and Obayashi, M. (2013) Subducted slabs stagnant above, penetrating through, and trapped below the 660 km discontinuity, Journal of Geophysical Research: Solid Earth, 118(11), 5920-5938.

Ghosh, S., and Schmidt, M.W. (2014) Melting of phase D in the lower mantle and implications for recycling and storage of H_2O in the deep mantle, Geochimica et Cosmochimica Acta, 145, 72-88.

Hacker, B.R. (2008) H_2O subduction beyond arcs, Geochemistry, Geophysics, Geosystems, 9(3).

Hirose, K., Takafuji, N., Sata, N., and Ohishi, Y. (2005) Phase transition and density of subducted MORB crust in the lower mantle, Earth and Planetary Science Letters, 237(1-2), 239-251.

Kaneshima, S. (2003) Small-scale heterogeneity at the top of the lower mantle around the Mariana slab, Earth and Planetary Science Letters, 209(1), 85-101.

Katsura, T., Yamada, H., Nishikawa, O., Song, M., Kubo, A., Shinmei,T., Yokoshi, S., Aizawa, Y., Yoshino, T. and Walter, M.J. (2004) Olivine–wadsleyite transition in the system $(Mg, Fe)_2SiO_4$. Journal of Geophysical Research, 109, B02209, doi:10.1029/2003JB002438.

Kawamoto, T. (2006) Hydrous phases and water transport in the subducting slab, Reviews in mineralogy and geochemistry, 62(1), 273-289.

King, S.D., Frost, D.J., and Rubie, D.C. (2015) Why cold slabs stagnate in the transition zone, Geology, 43(3), 231-234.

Litasov, K.D., and Ohtani, E. (2005) Phase relations in hydrous MORB at 18–28GPa: implications for heterogeneity of the lower mantle, Physics of the Earth and Planetary Interiors, 150(4), 239-263.

Litasov, K.D., Ohtani, E., Nishihara, Y., Suzuki, A., and Funakoshi, K. (2008) Thermal equation of state of Al‐and Fe‐bearing phase D, Journal of Geophysical Research: Solid Earth, 113(B8), B08205.

Litasov, K.D., Ohtani, E., Suzuki, A., and Funakoshi, K. (2007) The compressibility of Fe-and Al-bearing phase D to 30 GPa, Physics and Chemistry of Minerals, 34(3), 159-167.

Liu, X., Matsukage, K.N., Li, Y., Takahashi, E., Suzuki, T., and Xiong, X. (2018) Aqueous fluid connectivity in subducting oceanic crust at the mantle transition zone conditions. Journal of Geophysical Research-Solid Earth, 123(8), https://doi.org/10.1029/2018JB015973

Magni, V., Bouilhol, P., and van Hunen, J. (2014) Deep water recycling through time, Geochemistry, Geophysics, Geosystems, 15(11), 4203-4216.

Matsukage, K. N., Hashimoto, M., and Nishihara, Y. (2017) Morphological stability of hydrous liquid droplets at grain boundaries of eclogite minerals in the deep upper mantle, Journal of Mineralogical and Petrological Sciences, 112, 346-358, doi:10.2465/jmps.170309.

Matsuzaka, K., Akaogi, M., Suzuki, T., and Suda, T. (2000) Mg-Fe partitioning between silicate spinel and magnesiowüstite at high pressure: experimental determination and calculation of phase relations in the system Mg_2SiO_4-Fe_2SiO_4, Physics and Chemistry of Minerals, 27(5), 310-319, doi:10.1007/s002690050260.

Melekhova, E., Schmidt, M.W., Ulmer, P., and Pettke, T. (2007) The composition of liquids coexisting with dense hydrous magnesium silicates at 11–13.5 GPa and the endpoints of the solidi in the $MgO–SiO_2–H_2O$ system,

Geochimica et cosmochimica acta, 71(13), 3348-3360.
Nishi, M., Irifune, T., Tsuchiya, J., Tange, Y., Nishihara, Y., Fujino, K., and Higo, Y. (2014) Stability of hydrous silicate at high pressures and water transport to the deep lower mantle, Nature Geoscience, 7(3), 224-227.
Nishihara, Y., and Matsukage, K.N. (2016) Iron-titanium oxyhydroxides as water carriers in the Earth's deep mantle, American Mineralogist, 101(4), 919-927.
Ohira, I., Ohtani, E., Sakai, T., Miyahara, M., Hirao, N., Ohishi, Y., and Nishijima, M. (2014) Stability of a hydrous δ-phase, AlOOH–$MgSiO_2(OH)_2$, and a mechanism for water transport into the base of lower mantle, Earth and Planetary Science Letters, 401, 12-17.
Ohtani, E. (2015), Hydrous minerals and the storage of water in the deep mantle, Chemical Geology, 418(418), 6-15.
Ohtani, E., Mizobata, H., and Yurimoto, H. (2000), Stability of dense hydrous magnesium silicate phases in the systems Mg_2SiO_4-H_2O and $MgSiO_3$-H_2O at pressures up to 27 GPa, Physics and Chemistry of Minerals, 27(8), 533-544, doi:DOI 10.1007/s002690000097.
Okamoto, K., and Maruyama, S. (1999) The high-pressure synthesis of lawsonite in the MORB+ H_2O system, American Mineralogist, 84(3), 362-373.
Okamoto, K., and Maruyama, S. (2004) The eclogite–garnetite transformation in the MORB+H_2O system, Physics of the Earth and Planetary Interiors, 146(1), 283-296.
Ono, S., Mibe, K., and Yoshino, T. (2002) Aqueous fluid connectivity in pyrope aggregates: water transport into the deep mantle by a subducted oceanic crust without any hydrous minerals, Earth and Planetary Science Letters, 203(3-4), 895-903, doi:Pii S0012-821x(02)00920-2
Palin, R.M., and White, R.W. (2015), Emergence of blueschists on Earth linked to secular changes in oceanic crust composition, Nature Geoscience.
Pamato, M.G., Myhill, R., Ballaran, T.B., Frost, D.J., Heidelbach, F., and Miyajima, N. (2015) Lower-mantle water reservoir implied by the extreme stability of a hydrous aluminosilicate, Nature Geoscience, 8(1), 75-79.
Suzuki, A., Ohtani, E., and Kamada, T. (2000) A new hydrous phase δ-AlOOH synthesized at 21 GPa and 1000 C, Physics and Chemistry of Minerals, 27(10), 689-693.
Syracuse, E.M., van Keken, P.E., and Abers, G.A. (2010) The global range of subduction zone thermal models, Physics of the Earth and Planetary Interiors, 183(1), 73-90.
Takahashi, E. (1990) Speculations on the Archean mantle: missing link between komatiite and depleted garnet peridotite, Journal of Geophysical Research: Solid Earth, 95(B10), 15941-15954.
Yoshino, T., Nishihara, Y., and Karato, S. (2007) Complete wetting of olivine grain boundaries by a hydrous melt near the mantle transition zone, Earth and Planetary Science Letters, 256(3), 466-472.
Walter, M., Thomson, A., Wang, W., Lord, O., Ross, J., McMahon, S., Baron, M., Melekhova, E., Kleppe, A., and Kohn, S. (2015) The stability of hydrous silicates in Earth's lower mantle: Experimental constraints from the systems MgO–SiO_2–H_2O and MgO–Al_2O_3–SiO_2–H_2O, Chemical Geology, 418, 16-29.
Walter, M.J., Thibault, Y., Wei, K., and Luth, R.W. (1995) Characterizing Experimental Pressure and Temperature Conditions in Multi-Anvil Apparatus, Can J Phys, 73(5-6), 273-286.
Wang, X.-C., Wilde, S.A., Li, Q.-L., and Yang, Y.-N. (2015) Continental flood basalts derived from the hydrous mantle transition zone, Nature Communications, 6, 7700.
Zhang, J., Li, B., Utsumi, W., and Liebermann, R. (1996) In situ X-ray observations of the coesite-stishovite transition: reversed phase boundary and kinetics, Physics and Chemistry of Minerals, 23(1), 1-10.

This is a preprint, the final version is subject to change, of the American Mineralogist (MSA)
Cite as Authors (Year) Title. American Mineralogist, in press.
DOI: https://doi.org/10.2138/am-2019-6559

531 **Table 1.** Compositions of the starting materials (wt%) used in this study.

532

Starting material	JB-2* basalt	N-MORB
SiO_2	47.22	48.76
TiO_2	1.05	1.68
Al_2O_3	12.98	15.38
FeO	8.85	8.35
Fe_2O_3	2.95	0.93
MnO	0.19	0.18
MgO	11.93	8.27
CaO	8.78	11.51
Na_2O	1.81	2.71
K_2O	0.37	0.23
H_2O	3.50	2.00
Total	99.62	99.98

533

534

This is a preprint, the final version is subject to change, of the American Mineralogist (MSA)
Cite as Authors (Year) Title. American Mineralogist, in press.
DOI: https://doi.org/10.2138/am-2019-6559

535 **Table 2.** Experimental conditions and results.
536

Run NO.	T(℃)	P(GPa)	Duration (hours)	Run products
DHL-1	1000	17	24	Grt (81), Sti (10), Fe-Ti (4),Ti-CaPv (3), Mg-CaPv (1), fluid
DHL-4	1200	17	24	Grt (88), Sti (8), Ti-CaPv (3), fluid
DHL-7	900	18	36	Grt (68), Al-rich phase D (17), Na-rwd (2), Ti-CaPv (3), Fe-Ti (4), Sti (6), fluid
DHL-6	800	19	50	Grt (58), Al-rich phase D (23), Rwd(10), Mw (2), Hol (2), sti (5), fluid
DHL-5	1000	19	24	Grt (67), Al-rich phase D (18), Ti-CaPv (3), Rwd (5), Hol (3), Sti (4), fluid
DHL-19	1100	19	24	Grt (75), Fe-Ti (4), CaPv (6), Hol (2), Rwd(4), Sti (9), fluid
DHL-10	1200	19	13	Grt (82), Sti (8), Ti-CaPv (3), CaPv (1), Rwd (3), fluid
DHL-8	1000	20	27	Grt (64), Al-rich phase D (16), Ti-CaPv (3), CaPv (6), Hol (2), Mw (4), Sti (5), fluid
DHL-21	1000	20	33	Grt (69), Al-rich phase D (13), Ti-CaPv (1), CaPv (12), Hol (2), Sti (4), fluid
DHL-20	1000	23.1	24	Grt (43), Al-rich phase D (17), CaPv (18), Hol (3), Mw (9), Sti (10), fluid
DHL-22	1200	23.1	20	Grt (56), Al-rich phase D (13), CaPv (14), Sti (12), Mw (5), fluid
DHL-15	1000	25	24	Bdg (42), Al-rich phase H (15), CaPv (21), Hol (2), Mw (4), Sti (15), fluid
DHL-17	1200	25	12	Bdg (41), Al-rich phase H (17), CaPv (22), Mw (5), Sti (15),fluid
DHL-9	1000	26.3	24	Bgd (43), Al-rich phase H (15), CaPv (20), Sti (17), Mw (5), fluid

537

538 Abbreviations: grt, majoritic garnet; Fe-Ti, Fe-Ti oxyhydroxide; Ti-CaPv, Ti-rich Ca-perovskite;
539 rwd, ringwoodite; K-hol, K-hollandite; sti, stishovite; CaPv, Ca-perovskite; mw,
540 magnesiowustite; bdg, bridgmanite. The numbers in the parentheses are the proportions of run
541 products in wt%. The starting material used in run DHL-21 was hydrous N-MORB, whereas JB-
542 2* + brucite was used in other runs.

543

This is a preprint, the final version is subject to change, of the American Mineralogist (MSA)
Cite as Authors (Year) Title. American Mineralogist, in press.
DOI: https://doi.org/10.2138/am-2019-6559

544 **FIGURE CAPTIONS**

545

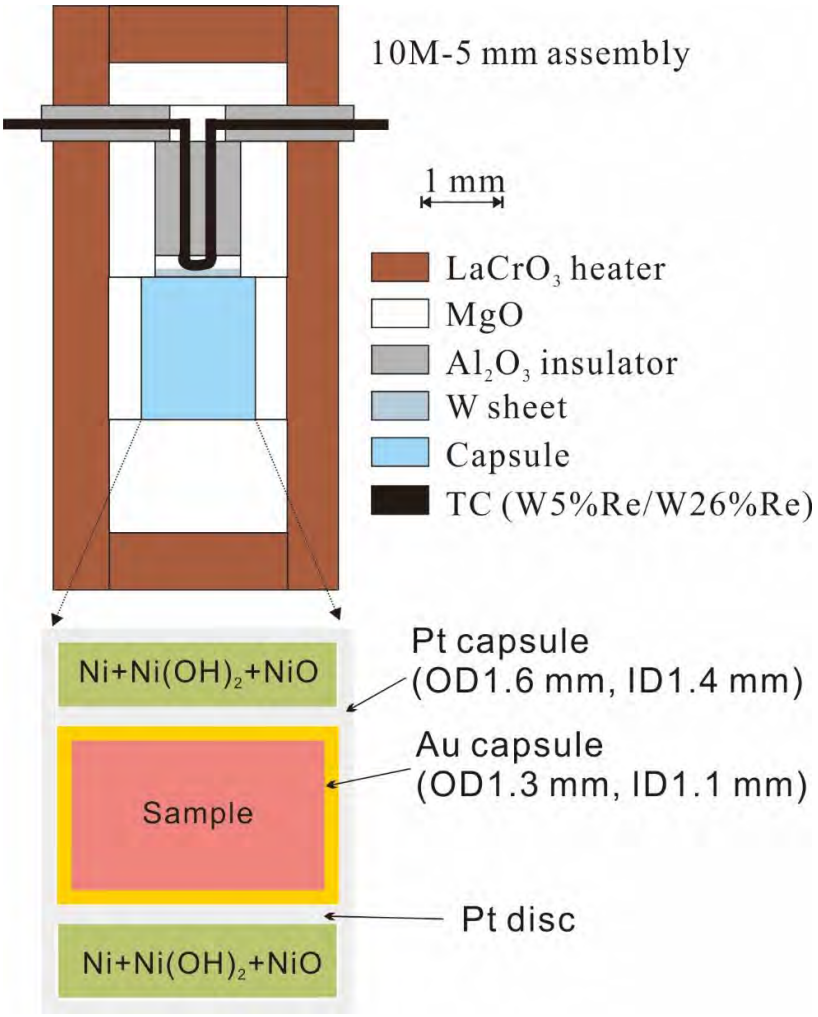

546
547

548 **Figure 1.** Schematic cross section of the cell assemblies used in runs at ≤20 GPa, in which a

549 double-capsule design was employed. A gold capsule was used as the sample container, and

550 oxygen fugacity was constrained to the Ni–NiO buffer. OD, outer diameter; ID, inner diameter.

551

This is a preprint, the final version is subject to change, of the American Mineralogist (MSA)
Cite as Authors (Year) Title. American Mineralogist, in press.
DOI: https://doi.org/10.2138/am-2019-6559

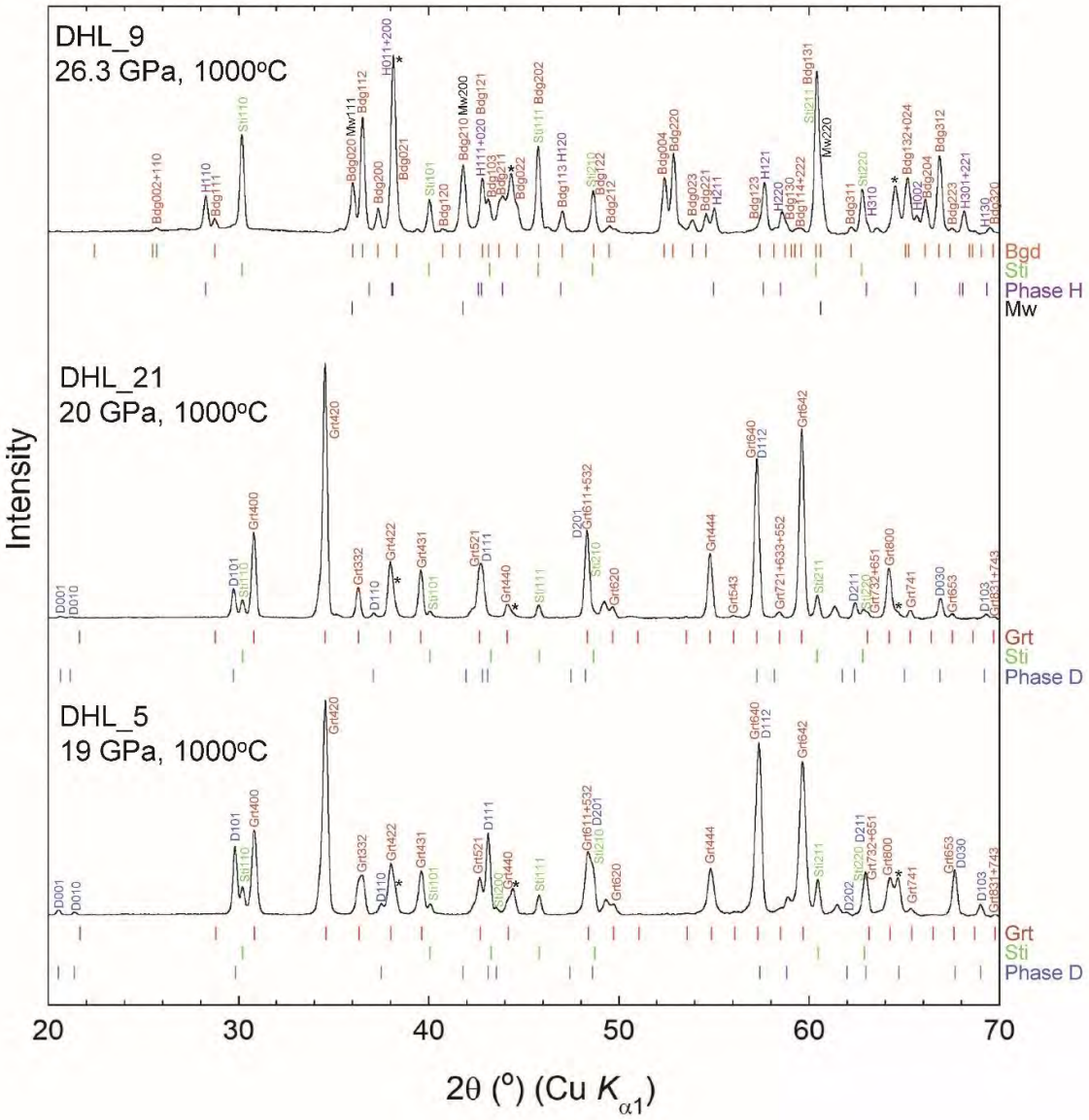

552
553 **Figure 2.** Selected X-ray diffraction patterns of the run products. Small bars indicate peak
554 position calculated from optimized lattice parameters for each phase. Space group of phase H is
555 assumed as $P2_1nm$ (Bindi et al., 2014).
556

This is a preprint, the final version is subject to change, of the American Mineralogist (MSA)
Cite as Authors (Year) Title. American Mineralogist, in press.
DOI: https://doi.org/10.2138/am-2019-6559

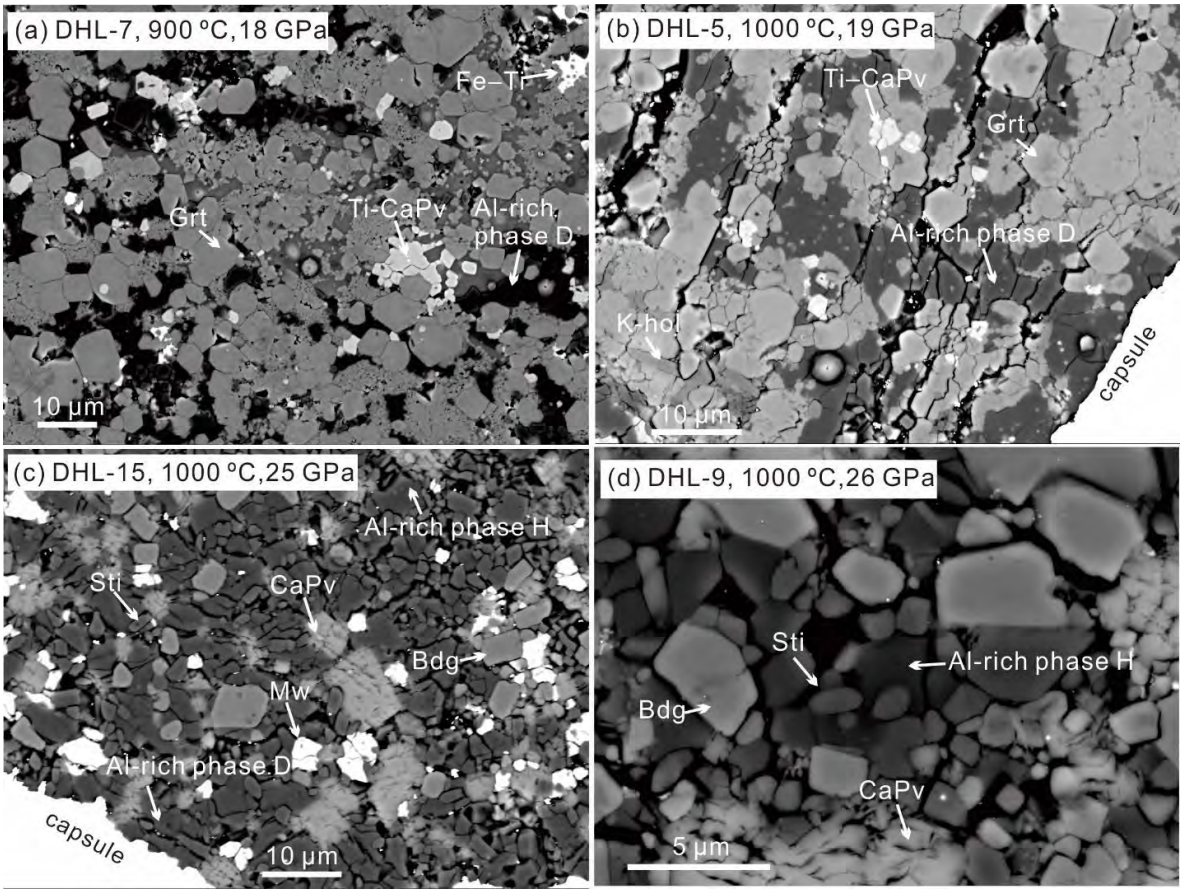

Figure 3. Back-scattered electron images of the representative charges. Phase abbreviations are as follows: Grt, majoritic garnet; Fe–Ti, Fe–Ti oxyhydroxide; Ti–CaPv, Ti-rich Ca-perovskite; K-hol, K-hollandite; Sti, stishovite; CaPv, Ca-perovskite; Mw, magnesiowustite; Bdg, bridgmanite.

This is a preprint, the final version is subject to change, of the American Mineralogist (MSA)
Cite as Authors (Year) Title. American Mineralogist, in press.
DOI: https://doi.org/10.2138/am-2019-6559

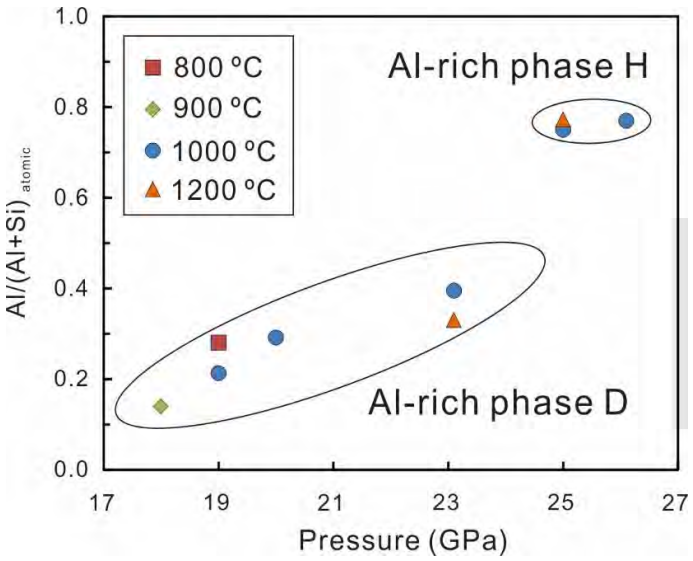

Figure 4. Compositions of Al-rich phase D and Al-rich phase H under various pressure–temperature conditions. The measured Al content in Al-rich phase D increased with increasing pressure and decreased with increasing temperature. Al-rich phase H contains more Al than Al-rich phase D.

This is a preprint, the final version is subject to change, of the American Mineralogist (MSA)
Cite as Authors (Year) Title. American Mineralogist, in press.
DOI: https://doi.org/10.2138/am-2019-6559

570

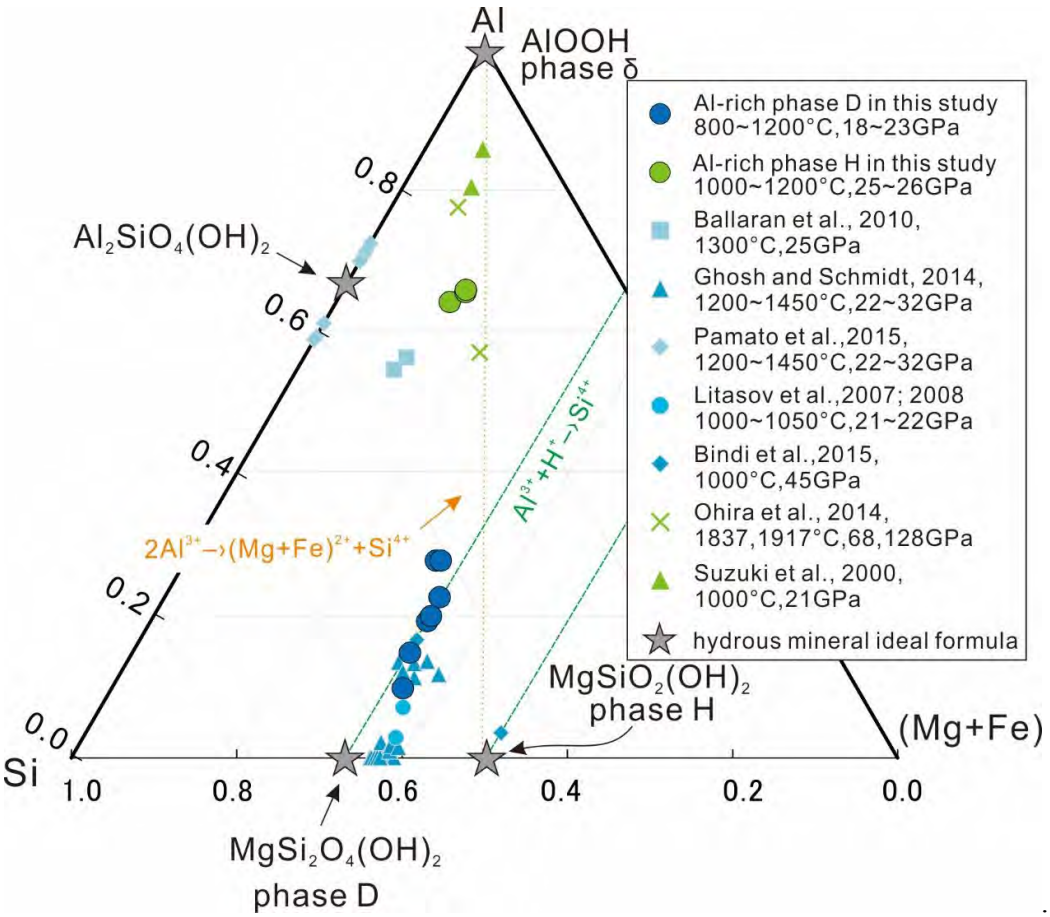

571

572 **Figure 5.** Compositions of Al-rich phase D and Al-rich phase H synthesized in this study and in
573 previous work performed with peridotitic and simplified systems, shown on a Si–Al–(Mg+Fe)
574 molar ternary diagram. Note that the binary Si-(Mg+Fe) is projected from the H_2O top in the
575 ternary H_2O-SiO_2-(Mg, Fe)O, modified from Walter et al. (2015, Fig. 1c). Gray stars show the
576 ideal formulae for various hydrous phases. Green dashed lines indicate the substitution of Al^{3+} +
577 H^+ for Si^{4+}. Al-rich phase H contains notably more Al than Al-rich phase D. Compositions of Al-
578 rich phase D and Al-rich phase H in this study (blue and green solid circles) are similar to those
579 of previous studies.

580

This is a preprint, the final version is subject to change, of the American Mineralogist (MSA)
Cite as Authors (Year) Title. American Mineralogist, in press.
DOI: https://doi.org/10.2138/am-2019-6559

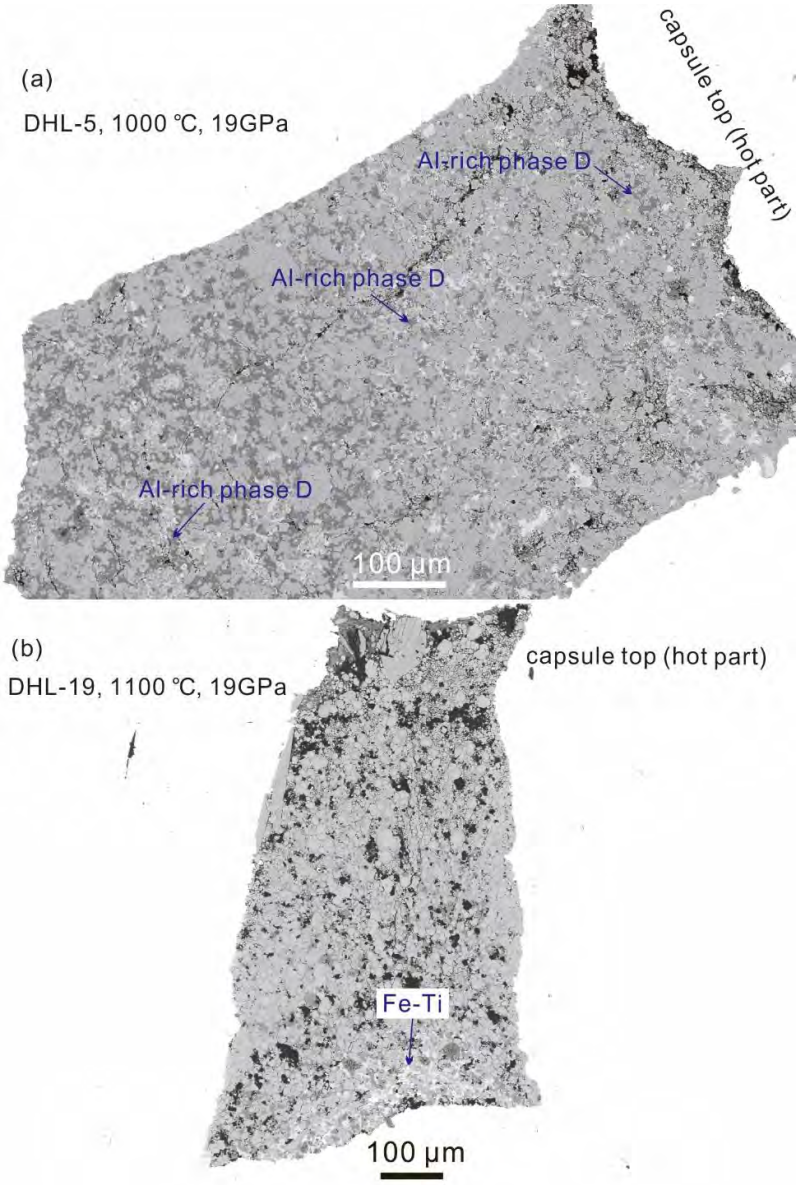

Figure 6. Distribution of hydrous phases in the run products from the experiments at the same pressure of 19 GPa but different temperatures. (a) Hydrous phase Al-rich phase D was present at the bottom and top of the capsule (1000 °C). (b) Only the hydrous phase Fe-Ti oxyhydroxide was present at the capsule bottom (1100 °C).

This is a preprint, the final version is subject to change, of the American Mineralogist (MSA)
Cite as Authors (Year) Title. American Mineralogist, in press.
DOI: https://doi.org/10.2138/am-2019-6559

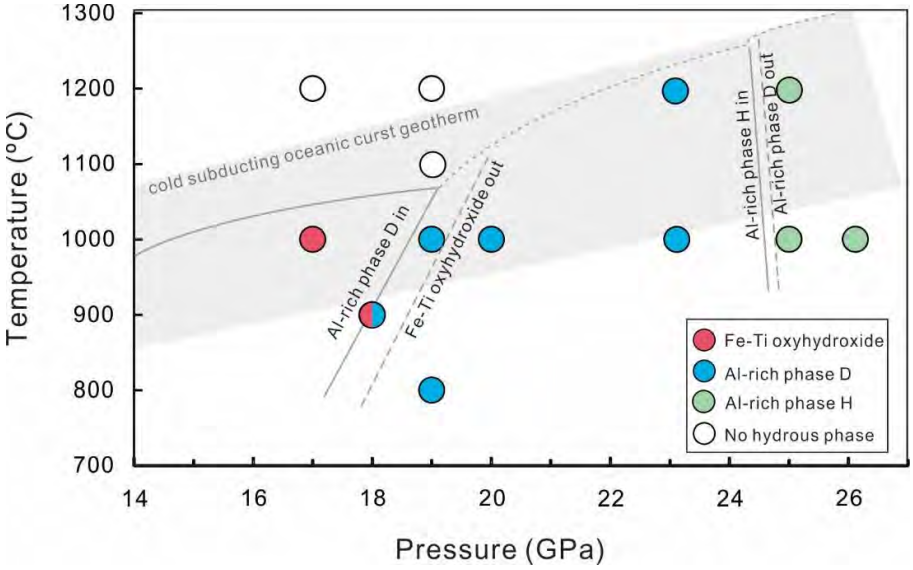

587

588 **Figure 7.** Pressure–temperature (P–T) stability fields of synthesized hydrous phases in basalt.
589 Gray curves outline the stability field of each hydrous phase, and the shaded area marks the P-T
590 range of cold subducting oceanic crust (Syracuse et al. 2010). Water can be sequentially stored in
591 the hydrous phases Fe–Ti oxyhydroxide, Al-rich phase D, and Al-rich phase H with increasing
592 pressure, making subducting oceanic crust a viable candidate for the transportation of surface
593 water into the lower mantle. No hydrous phase is stable at temperatures greater than 1100 °C and
594 pressures lower than 20 GPa. Note that Fe–Ti oxyhydroxide and Al-rich phase D coexist at 18
595 GPa and 900 °C. The pressure and temperature uncertainties are thought to be better than 1 GPa
596 and 50 °C.

597

This is a preprint, the final version is subject to change, of the American Mineralogist (MSA)
Cite as Authors (Year) Title. American Mineralogist, in press.
DOI: https://doi.org/10.2138/am-2019-6559

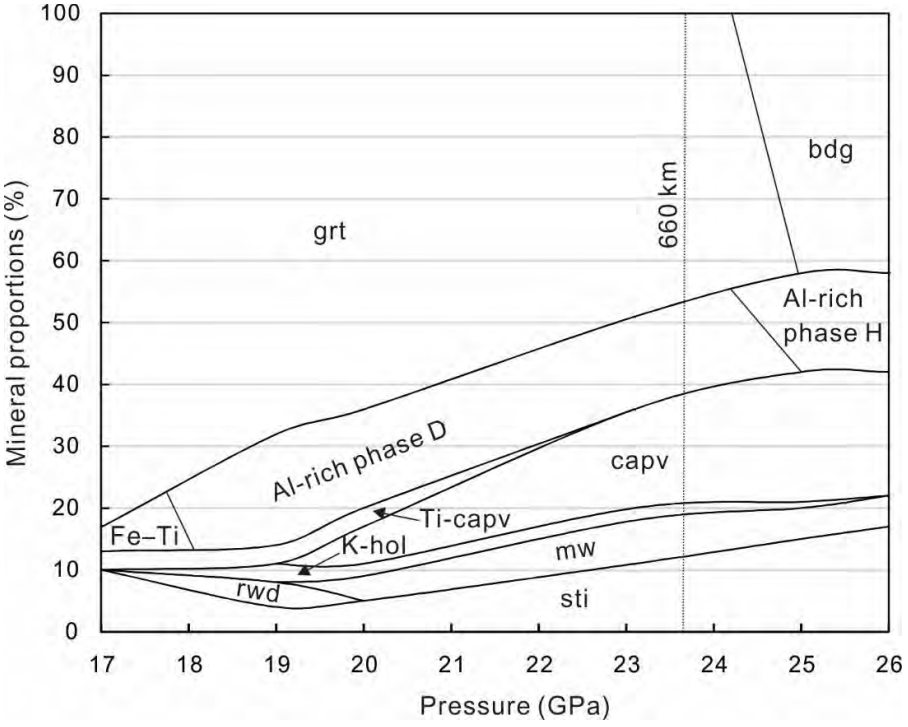

598

599 **Figure 8.** Phase proportion changes in cold subducting oceanic crust with depth. Phase

600 proportions are calculated based on data from a hydrous basalt + 3.5 wt% H_2O system in this

601 study. The slab geotherm is in the center of the shaded area in Fig. 7. See Fig. 3 for phase

602 abbreviations.

603

604

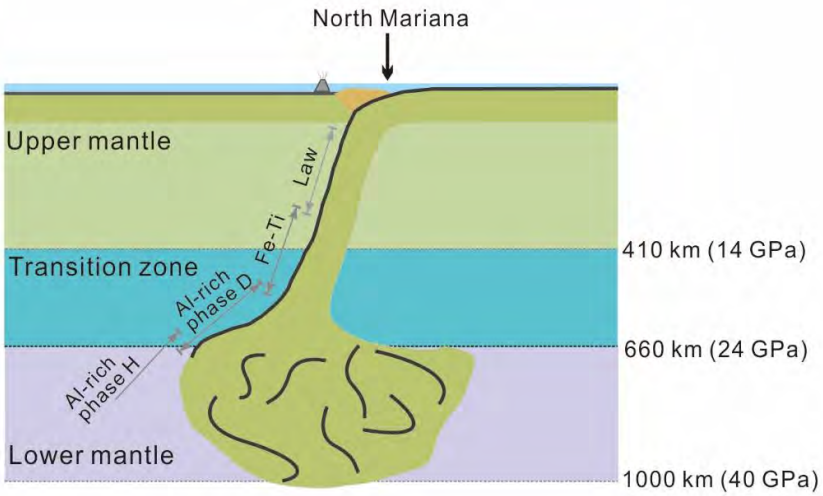

605
606 **Figure 9.** Schematic diagram of subduction in the North Mariana trench, according to
607 seismological observations (Fukao and Obayashi, 2013; Kaneshima, 2003). Subducted slabs
608 penetrate into the lower mantle and stagnate above a 1000-km depth. H_2O is stored in a
609 continuous chain of hydrous phases upon pressure increasing(lawsonite, Fe–Ti oxyhydroxide,
610 Al-rich phase D, and Al-rich phase H) in oceanic crust (black thin layer) at the top of a cold
611 subducting slab. Stagnant fragments of oceanic crust may thus be an important water reservoir in
612 the lower mantle. Abbreviations: Law, lawsonite; Fe–Ti, Fe–Ti oxyhydroxide.